

## Preparation of nanopores and their application for the detection of metals

D. Kaya, K. Kececi\*

<sup>1</sup>Department of Chemistry, Istanbul Medeniyet University, 34700, Istanbul, Turkey.

Submitted: June 1, 2017; Accepted: September 1, 2017

We have prepared nanopores with conical geometries and we have shown the translocation properties of poly(ethylene terephthalate) (PET) membranes. In order to obtain conically shaped nanopores, asymmetric etching procedure was followed. The characterization of PET membranes were performed by electrochemical methods and SEM measurements. The sensing was performed based on resistive-pulse sensing and current-potential (I-V) measurements. Finally, we have reported the resistive-pulse sensing of Ba<sup>2+</sup> using single nanoporous membranes and examined the potential dependence of resistive-pulse sensing. Effect of metal ion concentration on the ion - current rectification was also shown and it was concluded that a higher Ba<sup>2+</sup> concentration can be correlated with rectification ratios.

**Keywords:** Resistive-pulse sensing; track-etched nanopore; metal sensing; PET membrane

### INTRODUCTION

Resistive-pulse sensing, which is a powerful technique for the detection and analysis of molecules without labeling is an emerging field of research [1-3]. The resistive-pulse sensing paradigm was built on the well-known Coulter-counter principle, which was used to count particles and measure their sizes [4]. Basically, a pore (micron or sub-micron sized) is placed between two electrolyte solutions and particles are electrophoretically driven to the oppositely charged electrode. During the translocation of particles through the pore, the ionic current drops and this signal is used for counting particles and identifying their properties. This technique was miniaturized by using biological nanopores and enabled the detection of individual molecules without labelling and discriminate different types of molecules [5].

Several resistive-pulse studies have been conducted using biological nanopores, especially  $\alpha$ -Hemolysin [6, 7]. However, there are many shortcomings of biological nanopores which limit their efficiency as sensors such as their fixed size, instability and the fragility of the lipid bilayer in which the pore is placed. Therefore, chemically and mechanically robust synthetic nanopores were developed that are low cost, user friendly and enable highly sensitive and specific rapid analysis [8]. The precise control over the pore size and geometry, the ability to change the surface characteristics and to integrate with electronics or optical systems made the synthetic nanopores even more advantageous [9, 10]. Also, surface functionalization is more diverse in synthetic systems, which enhances the sensibility

and selectivity for certain molecules [11, 12].

Some of the techniques that are widely used for the fabrication of synthetic nanopores are electron beam lithography [13, 14], nanopipettes [15, 16], ion-beam sculpting [17], micromolding [18], and track-etching [19-22]. Compared to other nanopore fabrication techniques, track-etch method emerges as a viable alternative to obtain the desired nanopores in size and shape with uniform pore density without the limitations of the others [23].

In track-etch method membranes (or films) are first irradiated with accelerated heavy ions in order to create latent tracks inside the membranes. When the irradiated membranes are exposed to appropriate etching solution, the obtained tracks turn into nanopores and the etching process is controlled by neutralization of etching solution. If the polymer film is irradiated with a single-ion (i.e., 1 ion/membrane) and goes through chemical etching, single-pore membranes which are optimal for studying the detection and identification of individual molecules can be formed [24]. In track-etch method, some of the most widely used membranes are poly(ethylene terephthalate) (PET), polycarbonate (PC) and polyimide (PI). Different types of analytes such as proteins [25], DNAs [24, 26] etc. [27] have been detected using these polymer nanoporous membranes. Various nanopore geometries have also been reported in PET films which can affect the efficiency of sensing [28].

In this study, we showed the interaction of PET nanopores with divalent cations and monitor the real-time signals based on resistive-pulse sensing. The main reasons for choosing PET was that it is a mechanically and chemically stable, flexible material with a slightly negative surface charge.

\* To whom all correspondence should be sent.  
E-mail: kaan.kececi@medeniyet.edu.tr

Chemical etching of PET membranes leads to the formation of carboxylate groups ( $-\text{COO}^-$ ) on the surface of the membranes and pore walls [29]. The negative  $-\text{COO}^-$  groups on the walls of PET membrane had enhanced the affinity to cation analytes so in contrast to the previous studies, no chemical modification has been used on nanopore surface to promote the capture the cations. Successful stochastic sensing (resistive-pulse sensing) of divalent cations using  $\alpha$ -Hemolysin was previously shown by others [30-33].

## EXPERIMENTAL

### Materials and methods

PET membranes (3 cm diameter, 12  $\mu\text{m}$  thickness) were provided by Gesellschaft für Schwerionenforschung (GSI, Darmstadt-Germany). The membranes were irradiated with heavy ions (i.e., Au ion, 11.4 MeV) at various ion densities even down to 1 ion/membrane. This was succeeded by defocusing the ion beam and using a metal mask with a 0.1 mm diameter aperture with a shutter system which shuts down the ion beam as the single ion passage was detected. All the membranes were exposed to UV irradiation overnight ( $\lambda = 320 \text{ nm}$ ) to saturate the damages in tracks. All solutions were prepared from deionized water (Millipore Direct-Q 5, Millipore Co.). Formic acid ( $\text{HCOOH}$ ), sodium hydroxide ( $\text{NaOH}$ ), barium chloride ( $\text{BaCl}_2$ ) and potassium chloride ( $\text{KCl}$ ) were purchased from Sigma Aldrich. All chemicals were used as received without further purification.

### Preparation of nanopore membranes

Prior to etching, membranes were treated with long-wave UV irradiation overnight in order to increase the track etching rate and make the pores more homogeneous in size by sensitizing the tracks. Conically shaped nanopores were obtained using asymmetric chemical etching whose conditions were previously discussed [34]. Shortly, the membrane was placed in a conductivity cell with one side of the cell facing the UV-treated side of the membrane, filled with alkaline etching solution (9 M  $\text{NaOH}$ ) and the other half-cell was filled with the stopping solution (1 M  $\text{HCOOH}$  and 1 M  $\text{KCl}$ ). Platinum ( $\text{Pt}$ ) electrodes were immersed into each cell and 1 V transmembrane potential was applied to monitor the breakthrough moment. The etching process was continued for two hours and then the etching solution was replaced with stopping solution for neutralization. Then both cells were rinsed with di-water to remove possible residues from the membrane surface. After this etching process, a conically shaped nanopore was obtained with two

different sized openings called base (large opening) and tip (small opening).

### Characterization of the nanopores

The large opening of the nanopore ( $d_{\text{base}}$ ) was determined by the SEM images of multipore membranes ( $10^8$  nanopores/ $\text{cm}^2$ ). Single pore membranes were etched under the same conditions as multipore membranes and the small opening ( $d_{\text{tip}}$ ) was determined through electrochemical measurements [12]. For the electrochemical measurement, each side of the conductivity cell was filled with electrolyte solution (i.e., 1 M  $\text{KCl}$ , 10 mM PBS buffer at  $\text{pH} = 7$ ).  $\text{Ag}/\text{AgCl}$  electrodes (BAS, West Lafayette, IN) were immersed into both sides of the cell and potential was stepped (50 mV) between -1 V and +1 V (Keithley 6487 picoammeter/voltage source, Cleveland, OH, USA). Since the resistance of the nanopore ( $R$ ) is proportional to the conductivity of solution ( $\rho$ ), the length of nanopore ( $L$ , thickness of the membrane),  $d_{\text{base}}$  and  $d_{\text{tip}}$ ; the tip diameter ( $d_{\text{tip}}$ ) can be calculated with Eqn. 1.  $R$  value was calculated from the reciprocal of the slope of the current – voltage ( $I$ - $V$ ) curve [34]. The average of three sequential measurements was used for the calculations.

$$R = \frac{4\rho L}{\pi d_{\text{tip}} d_{\text{base}}} \quad (1)$$

The conductivity of the solution was measured using a conductivity meter (Mettler-Toledo FE 30, Columbus, OH, USA).

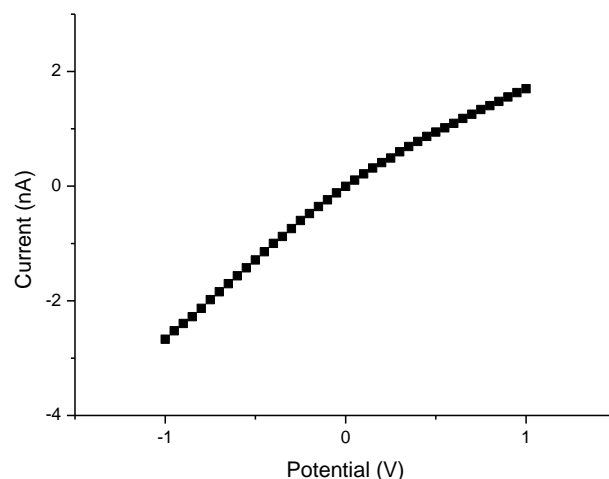


**Fig. 1.** I-V Curve of a PET single conical nanopore in 1 M  $\text{KCl}$  ( $d_{\text{base}}$ : 515 nm;  $d_{\text{tip}}$ : 6 nm).

### Electroless gold plating

The formation of gold replicas inside the nanopores by electroless gold plating method, which is a templating technique, gives valuable information about the geometry of the nanopore. This is simply achieved by filling the pores with Au and removing

the polymer template by dissolving it. The exact geometry of the replicas obtained from multiporous membranes can be visualized using SEM. The schematic representation of chemical plating of the nanopore wall is given in Fig. 2. The process mainly consists of three steps. Firstly  $\text{Sn}^{2+}$  is coated on the negatively charged pore wall of PET. After washing the membrane with methanol, it is immersed in the  $\text{AgNO}_3$  solution containing ammonia to form a redox reaction on the pore wall of the membrane where Ag (I) is converted to elemental Ag while Sn (II) is oxidized to Sn (IV). The gold coating solution contains  $\text{Na}_3\text{Au}(\text{SO}_3)_2$ ,  $\text{Na}_2\text{SO}_3$ ,  $\text{NaHCO}_3$  and formaldehyde in various proportions. When the membrane is immersed in this solution, once more a redox reaction occurs on the pore wall. Since gold has a more positive reduction potential than silver, the gold particles switch place with the silver on the surface. These gold particles serve as catalysts in the presence of formaldehyde, thereby reducing the Au (I) ions to Au (0). After Au deposition into the nanopores, the membrane was dissolved and the remaining gold nanocones were filtered with a Whatman Anodisc membrane. The obtained nanocones were investigated with SEM.

#### Resistive-pulse sensing experiments

The chemically etched nanopore membrane was placed between two halves of a conductivity cell and each half-cell was filled with 100 mM KCl.

Background current-time measurements were recorded between (+1000 mV) – (-1000 mV) with 100 mV steps. Cation analytes at predetermined concentrations were added to the tip side of the conductivity cell. Ag/AgCl electrodes were used to measure the current-pulses (events). An Axopatch 200B (Molecular Devices Corporation, CA, USA) was used in voltage-clamp mode to apply a transmembrane potential between Ag/AgCl electrodes with a low-pass Bessel filter at 2 kHz bandwidth. The signal was digitized using a Digidata 1440 analog-to-digital converter (Molecular Devices Corporation, CA, USA) at a sampling frequency of 5 kHz. Data were analyzed using pClamp 10.5 (Molecular Devices Corporation).

## RESULTS AND DISCUSSION

### Characterization of the nanopores

PET membranes were etched with alkali solution (i.e., 9M NaOH) from one side only for a conical geometry. After the etching process, the base diameters of conical nanopores were determined by SEM images of these multipore membranes (average of minimum 10 pores) (Figure 3). The base diameter of the conical membranes etched for 2 hours was found to be  $533 \pm 46$  nm.

The conical geometry of the pores was confirmed using the SEM images of gold nanocones obtained with electroless gold plating method (Fig. 4).

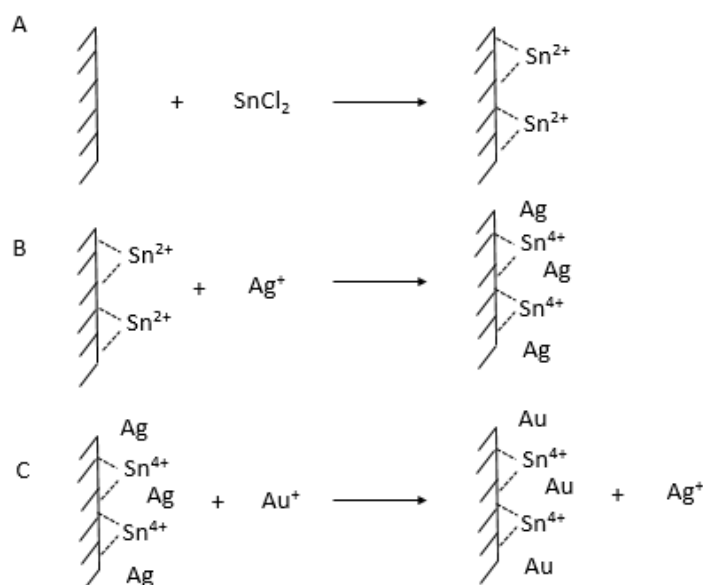
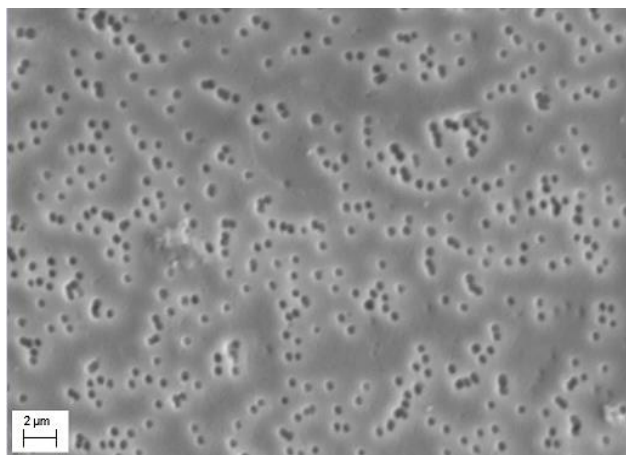
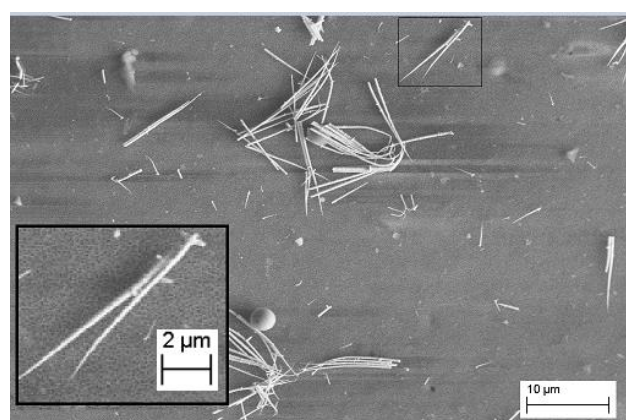


Fig. 2. Au plating steps of the nanopore surface.



**Fig. 3.** SEM image of multi-porous PET membrane etched for 2 hours.



**Fig. 4.** SEM image of Au cone replicas by template synthesis

#### Resistive-pulse sensing of $Ba^{2+}$ ions

In order to examine the transport properties of  $Ba^{2+}$  ions, potential dependence of the current-pulses and effect of ion concentration on the current rectification were studied. The current was recorded with 100 mM KCl at 400 mV before adding the metal analyte and was found to be stable, showing no current-pulses (Fig. 5 - A). When the  $Ba^{2+}$  ions (10 mM in 100 mM KCl) were added to the tip side of the membrane, current-pulses were observed under same potential due to the translocation of the metal ions (Fig. 5 - B). The current-pulse signals of  $Ba^{2+}$  showed an upward trend due to the higher binding affinity to carboxylate groups on the surface, decreasing the overall resistance of the pore. These conductive pulses can also be attributed to the high conductance of the particles relative to the electrolyte and the effect of particle charge on the ionic distribution near the pore opening, increasing the conductance temporarily [35].

The potential was stepped down to 250 mV and no current pulses were observed below this value (Fig. 5 - C-E).

The potential dependence of  $Ba^{2+}$  translocation is given in Fig. 6. The current-pulse frequency was calculated by averaging the number of current-pulses of three 5 minute current-time recordings and a linear correlation was observed between the examined potential values. A similar linear potential dependency was shown for DNA translocation in various studies [34, 36]. Harrell and co-workers have explained the translocation phenomenon in track-etched nanoporous membranes in detail [36] and they have derived an equation (Eqn. 2) giving the relationship between the frequency of current-pulses ( $f$ ) and electric field ( $E$ ) where,  $z$  is the charge of the analyte,  $D_t$  is the diffusion coefficient,  $C$  is the concentration and  $A$  is the Avogadro's number.

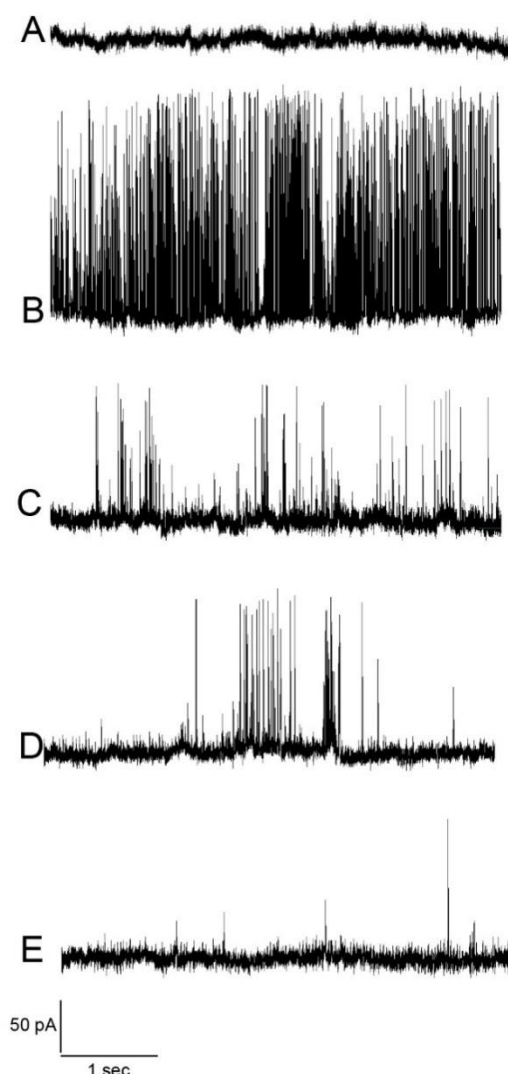


**Fig. 5.** Current-time traces of  $Ba^{2+}$  (10 mM) at 400 mV (without analyte) (A), 400 mV (B), 350 mV (C), 300 mV (D), 250 mV (E) Tip diameter = 6 nm.

$$f = -zFD_tCE(\pi r_{tip}^2)A/RT \quad (2)$$

According to previous studies, for conically shaped track-etched nanopores, the electric field strength (E) ranges between 1.3 and 2 MV/m [37], which forms a trapping zone to capture the molecule easily at the tip [38]. So the increase in the electric field at the nanopore entrance causes a linear increase in the current-pulse frequency. The linear dependence to potential and the occurrence of a threshold voltage suggest that the current-pulse frequency was dominated by the transport of Ba<sup>2+</sup> ions through the nanopore.

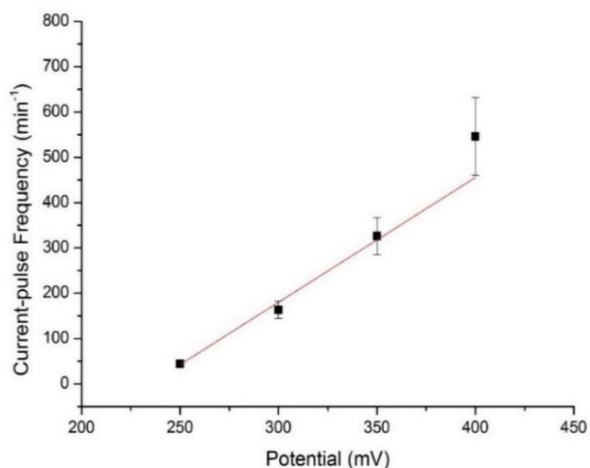


**Fig. 6.** Current-pulse frequency versus potential (10 mM Ba<sup>2+</sup>).

#### Effect of concentration on ion current rectification

It has previously been discussed by Siwy that asymmetric nanopores cause rectification on the ionic current even though the concentration of the

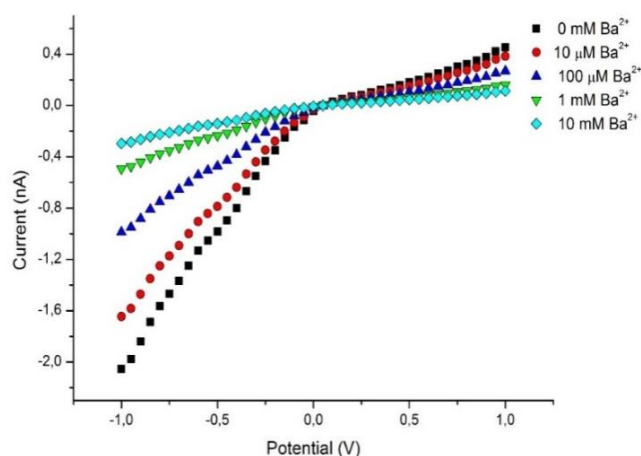


**Fig. 7.** I-V plots of Ba<sup>2+</sup> at various concentrations (Tip diameter = 5 nm).

electrolyte on both sides of the nanopore are the same and as a result asymmetric I-V curves are observed [39]. This non-linear behavior which is dependent on the surface charge can be described as the ‘on’ and ‘off’ state of the nanopore.

The ion current rectification (ICR) is the ratio between the current values at -1 V and +1 V (see Eqn. 3). PET nanopores have a negative surface charge at neutral pH due to the carboxylate groups produced during etching and at neutral pH the ICR is expected to be higher than 1 as the nanopore surface charge is negative.

$$ICR = \frac{|i_{-1}|}{|i_{+1}|} \quad (3)$$

In order to investigate the effect of Ba<sup>2+</sup> concentration on the ion current rectification, a series of Ba<sup>2+</sup> solutions at varying concentrations (10 μM – 10 mM) were prepared in 100 mM KCl. I-V curves obtained with Ba<sup>2+</sup> solutions at different concentrations are presented in Fig. 7.

Ion- current rectification ratios were calculated and plotted against log [Ba<sup>2+</sup>] values in order to further examine the effect of analyte concentration on the rectification behaviour (Fig. 8). It is shown that a decrease in ICR was observed with increasing Ba<sup>2+</sup> concentrations. This finding indicates that through the interactions between the negatively charged pore surface and positive Ba<sup>2+</sup> ions, the surface charge was decreased and ICR decreased accordingly since the I-V curves are able to give information about the surface charge on the pore walls. A similar behaviour was shown by Zhai et.al. for a conical PET nanopore for Cr<sup>3+</sup> detection [40].

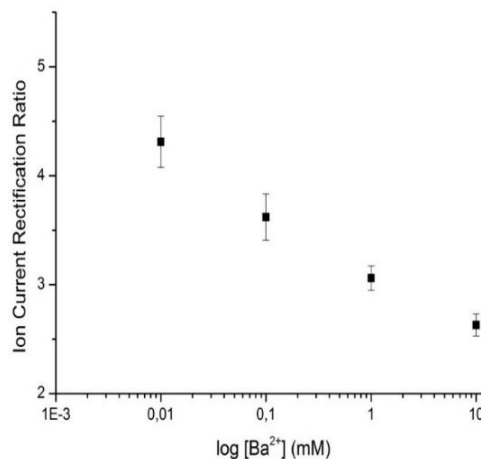


**Fig. 8.** Dependence of ion current rectification ratio on Ba<sup>2+</sup> concentration.

## CONCLUSION

In this work, track-etched PET membranes were used to fabricate asymmetric nanopores with conical

geometries. The potential use of these nanoporous membranes as resistive-pulse sensor for metal ions was shown and Ba<sup>2+</sup> ion was chosen as model showed the only resistive-pulse signal and correlation of metal ion (i.e., Ba<sup>2+</sup>) using track-etched polymer membranes. The current-pulse frequency had a linear dependence on applied potential. This linear dependence to potential indicated that the current-pulse frequency was dominated by the transport of Ba<sup>2+</sup> ions through the nanopore. Ion-current rectification ratios were calculated and their dependence to Ba<sup>2+</sup> concentration was also investigated. The opposite correlation between Ba<sup>2+</sup> and ICR was shown. This was due to the interactions between the negatively charged pore surface and positive Ba<sup>2+</sup> ions, decreasing the overall surface charge and ICR accordingly.

**Acknowledgement.** This work is financially supported by Istanbul Medeniyet University Scientific Research Projects Coordination Unit (Project Number: FKD-2015-432)

#### REFERENCES

1. B.M. Venkatesan, R. Bashir, *Nature Nanotechnol.*, **6**, 615 (2011).
2. Y.R. Kim, J. Min, I.H. Lee, S. Kim, A.G. Kim, K. Kim, K. Namkoong, C. Ko, *Biosensors Bioelectronics*, **22**, 2926 (2007).
3. M. AdelaBooth, R. Vogel, J.M. Curran, S. Harbison, J. Travas-Sejdic, *Biosensors Bioelectronics*, **45**, 136 (2013).
4. W.H. Coulter, Means for Counting Particles Suspended in a Fluid, U. Patent, Editor. 1953, USA.
5. J.J. Kasianowicz, E. Brandin, D. Branton, D.W. Deamer, *Proc. Natl. Acad. Sci. USA*, **93**, 13770 (1996).
6. J. Chu, M. Gonzalez-Lopez, S.L. Cockroft, M. Amorin, M.R. Ghadiri, *Angew Chem Int Edit*, **49**, 10106 (2010).
7. J.Schmidt, *Curr. Opinion Biotechnol.*, **39**, 17 (2016).
8. M. Kuhnemund, M. Nilsson, *Biosens Bioelectron*, (2014).
9. D. Kaya, A. Dinler, N. San, K. Kececi, *Electrochimica Acta*, **202**, 157 (2016).
10. R. Patricio, A. PavelYu, C. Javier, M. Salvador, *Nanotechnology*, **19**, 315707 (2008).
11. S.M. Iqbal, D. Akin, R. Bashir, *Nat Nanotechnol*, **2**, 243 (2007).
12. K. Kececi, L.T. Sexton, F. Buyukserin, C.R. Martin, *Nanomedicine-UK*, **3**, 787 (2008).
13. A.J. Storm, J.H. Chen, X.S. Ling, H.W. Zandbergen, C. Dekker, *Nature Materials*, **2**, 537 (2003).
14. Y. Liebes-Peer, V. Bandalo, Ü. Sökmen, M. Tornow, N. Ashkenasy, *Microchim Acta*, **183**, 987 (2016).
15. Y.X. Wang, K. Kececi, M.V. Mirkin, V. Mani, N. Sardesai, J.F. Rusling, *Chem Sci*, **4**, 655 (2013).
16. C.A. Morris, A.K. Friedman, L.A. Baker, *Analyst*, **135**, 2190 (2010).
17. A.L. Biance, J. Gierak, É. Bourhis, A. Madouri, X. Lafosse, G. Patriarche, G. Oukhaled, C. Ulysse, J.C. Galas, Y. Chen, L. Auvray, *Microelectronic Engineering*, **83**, 1474 (2006).
18. O.A. Saleh, L.L. Sohn, *Nano Letters*, **3**, 37 (2003).
19. L.X. Cao, Y.G. Wang, *Radiat Meas*, **44**, 1093 (2009).
20. T.W. Cornelius, B. Schiedt, D. Severin, G. Pepy, M. Toulemonde, P.Y. Apel, P. Boesecke, C. Trautmann, *Nanotechnology*, **21** (15) (2010).
21. Q.H. Nguyen, M. Ali, R. Neumann, W. Ensinger, *Sensors and Actuators B-Chemical*, **162**, 216 (2012).
22. J. Wang, C.R. Martin, *Nanomed*, **3**, 13 (2008).
23. A. Kocer, L. Tauk, P. Dejardin, *Biosensors Bioelectronics*, **38**, 1 (2012).
24. A. Mara, Z. Siwy, C. Trautmann, J. Wan, F. Kamme, *NanoLetters*, **4**, 497 (2004).
25. Z. Siwy, L. Trofin, P. Kohli, L.A. Baker, C. Trautmann, C.R. Martin, *JACS*, **127**, 5000 (2005).
26. B. Schiedt, K. Healy, A.P. Morrison, R. Neumann, Z. Siwy, *Nuclear Instruments and Methods in Physics Research Section B: Beam Interactions with Materials and Atoms*, **236**, 109 (2005).
27. E.A. Heins, Z.S. Siwy, L.A. Baker, C.R. Martin, *NanoLett*, **5**, 1824 (2005).
28. P.Y. Apel, I.V. Blonskaya, S.N. Dmitriev, O.L. Orelovich, B.A. Sartowska, *Nuclear Instruments and Methods in Physics Research Section B: Beam Interactions with Materials and Atoms*, **365, Part A**, 409 (2015).
29. Z. Siwy, P. Apel, D. Baur, D.D. Dobrev, Y.E. Korchev, R. Neumann, R. Spohr, C. Trautmann, K.O. Voss, *Surface Science*, **532**, 1061 (2003).
30. O. Braha, L.Q. Gu, L. Zhou, X. Lu, S. Cheley, H. Bayley, *NatBiotechnol*, **18**, 1005 (2000).
31. S. Wen, T. Zeng, L. Liu, K. Zhao, Y. Zhao, X. Liu, H.-C. Wu, *J AmChemSoc*, **133**, 18312 (2011).
32. C. Yang, L. Liu, T. Zeng, D. Yang, Z. Yao, Y. Zhao, H.-C. Wu, *Anal. Chem.*, **85**, 7302 (2013).
33. H.-Y. Wang, Z.-Y. Song, H.-S. Zhang, S.-P. Chen, *Microchim Acta*, **183**, 1003 (2016).
34. K. Kececi, N. San, D. Kaya, *Talanta*, **144**, 268 (2015).
35. E. Weatherall, G.R. Willmott, *The Journal of Physical Chemistry B*, **119**, 5328 (2015).
36. C.C. Harrell, Y. Choi, L.P. Horne, L.A. Baker, Z.S. Siwy, C.R. Martin, *Langmuir*, **22**, 10837 (2006).
37. L.T. Sexton, L.P. Horne, S.A. Sherrill, G.W. Bishop, L.A. Baker, C.R. Martin, *JACS*, **129**, 13144 (2007).
38. S. Lee, Y. Zhang, H.S. White, C.C. Harrell, C.R. Martin, *Anal Chem*, **76**, 6108 (2004).
39. Z.S. Siwy, *Adv. Funct. Mater.*, **16**, 735 (2006).
40. Q. Zhai, J. Wang, H. Jiang, Q. Wei, E. Wang, *Talanta*, **140**, 219 (2015).